Reprinted from

Symposium on

Machine Processing of

Remotely Sensed Data

June 21 - 23, 1977

The Laboratory for Applications of
Remote Sensing

Purdue University
West Lafayette
Indiana

IEEE Catalog No.
77CH1218-7 MPRSD

A PRACTICAL METHOD FOR CORRECTING BIDIRECTIONAL REFLECTANCE VARIATIONS

DWIGHT D. EGBERT
General Telephone Electronics/Information Systems

I. ABSTRACT

The purpose of the investigation described here was to analyze angular bidirectional reflectance variations and test the hypothesis that first order variations could be described from a consideration of shadows created by surface perturbations. The results reported here demonstrate the validity of this approach, and while it is not suitable for calculating absolute spectral reflectance characteristics, the development of such a model was not the objective of the investigation since other models already exist for these calculations. Instead, a model was needed which can make relative angular corrections to bidirectional reflectance measurements independent of the details of surface geometry. The theoretical model derived in this investigation from an analysis of shadow formation is such a model.

II. INTRODUCTION

This paper presents the results of the study of a new approach for predicting angular reflectance variations of very rough surfaces in the visible and near infrared region of the electromagnetic spectrum.

Other studies attempting to predict angular variations in reflectance (Suits, 1972; Smith and Oliver, 1972) are based upon extensions of the Allen, Gayle, and Richardson (1970) canopy model. The resulting models have proven reasonably successful for certain vegetation canopies and indirectly take into account some shadowing effects. Hapke (1963), alternatively, started with a similar model and altered it significantly to take into account a preferred scatter direction caused by obstructions. This alteration allowed the shadowing obstructions to greatly influence the resulting reflectance vs. angle functions. Hapke's model agreed very closely with experimental results (Hapke and Van Horn, 1963) for several porous surfaces.

The approach taken here starts with the assumption that shadowing parameters are first order determinants of angular reflectance variations.

From this viewpoint a new model was developed to predict these angular variations rather than trying to bend the older model into a form to allow adequate influence of the shadowing parameters. Experimental reflectance measurements were made for several laboratory model surfaces as well as "real-world" surfaces under controlled angular illumination conditions. The surface geometrical roughness properties were measured to provide input parameters for the reflectance model. The reflectance variations predicted by the model were then compared with the experimental measurements to test for statistically significant correlation.

The results of the investigation demonstrated that for both laboratory and field experiments, two factors explain the majority of the bidirectional reflectance variation.

(1) When a surface is illuminated by a collimated constant intensity light source, 85 to 90 percent of the bidirectional reflectance variance is explained by the cosine of the illumination incidence angle.

(2) A consideration of shadowing explains 80 to 85 percent of the remaining bidirectional reflectance variance.

It was found that the model worked quite well with only two input parameters to describe the surface geometry.

(1) average number of perturbations per unit area

(2) average perturbation size

It is significant that the theoretical shadow model derived for ideal perturbation shapes accurately predicts reflectance variations for natural surfaces with irregularly shaped perturbations. This demonstrates that total shadow area, and the rate of change of this area with angle, are independent of the exact shape of surface perturbations. Thus, an operational reflectance correction model is feasible which will not require detailed information about surface geometry as input.

III. APPROACH

The classical approach for calculating the reflection of electromagnetic waves from surface boundaries typically utilizes one of two ideal types of surfaces. The first is an ideal specular reflecting surface, and the second is an ideal diffuse or Lambertian surface. For precisely described surface geometries, the reflection properties of any surface can be exactly calculated using this classical approach. However, the precise description of the surface geometry which is required may include microscopic surface irregularities, and the approach may produce equations of such length and complexity that solution is impractical.

The types of surfaces of interest in remote sensing are neither ideally specular nor ideally diffuse. Also, if a theoretical model describing the angular reflectance variations of these surfaces is to be useful, it must be relatively independent of precise surface geometries. The approach to describing these surfaces which is taken here is to approximate the reflectance variations with a superposition of a specular term with a diffuse term. Both of these terms are modulated by a shadow function which is the primary factor in this model. For most surfaces of interest, the specular term will be small but not negligible, especially at large incidence illumination and viewing angles.

The interaction between the shadow function and the other terms is demonstrated with a qualitative example consisting of a nearly Lambertian plane surface upon which spherical perturbations are placed. First, consider looking within a surface area dA from some arbitrary, but fixed, direction while varying the incidence illumination angle. For example, while looking vertically down on the surface, the following changes can be seen. If the surface is illuminated vertically (i.e., $\theta_i = 0$), no shadows appear and primarily diffuse reflectance is observed for both plane and perturbations over the entire area dA as shown in Figure 1a. Now, as θ_i is allowed to change to some non-zero value (e.g., 30°), the appearance of the surface is broken up into primarily diffuse reflecting areas interspersed with shadow areas of essentially zero reflectance as shown in Figure 1b. Further, if θ_i is allowed to increase to a larger value (e.g., 60°), the appearance of the surface will change to include more and larger shadow areas as shown in Figure 1c.

From this example, it is clear that the single reflectance value measured by a remote sensing system, integrated over the entire surface area dA, will be proportional to the fraction of dA which is not in shadow. Thus, in order to describe the bidirectional reflectance, it is only necessary to calculate the fraction of dA which is not in shadow for any given set of incidence illumination angle, incidence look angle, and azimuth angle. This modified area is then multiplied by a constant for the plane and by the Lambertian reflectance pattern

for the spheres. For this example, the specular terms are very small, but they are also included in a similar manner.

Even from this viewpoint, an exact calculation of the shadow area requires a detailed knowledge of the surface geometrical properties. However, it was hypothesized that statistically the total shadow area within dA, and more importantly the change of shadow area with angle, would be dependent not on the exact shapes of the perturbations, but rather on gross average geometrical parameters. This hypothesis was confirmed during the detailed laboratory experiments performed as a part of this investigation. Visually, this behavior is apparent in Figure 2, which shows vertical views of several different objects and their shadows under three different angles of illumination. To a good approximation, the areas of the shadows cast on the horizontal plane as well as the rate of change of these shadow areas are primarily determined by the objects' heights and widths rather than by their detailed shapes. Thus, it is to be expected that over the surface area dA, the shadow controlling parameters will be a) average perturbation height, b) average perturbation width, and c) total number of perturbations within dA (i.e., perturbation density). Also, to a good approximation, the Lambertian reflectance patterns for ideal perturbations such as spheres, ellipses, and cylinders (which are well known) can be used to describe the patterns of more irregular perturbations. This is possible because the entire ensemble of perturbations within dA is considered as a single quantity.

As a result of these considerations, the approach in this investigation has been to start with an analysis of artificially prepared surfaces and proceed to the analysis of "real-world" surfaces in the following manner. First, two different model surfaces (spherical perturbations and vertical cylinder perturbations) were chosen as being reasonably representative of real surfaces. Nine model surfaces of each of the two types were generated with different values of perturbation size and density distributions. Laboratory models were constructed for each surface and exact mathematical descriptions for shadow and reflectance behavior were developed for each of the two types of perturbations. Measurements of reflectance were made under a controlled range of 432 different angular conditions for each surface. Then, the appropriate distribution parameters were input to the appropriate mathematical model and the predicted reflectance values compared with the measured values.

Particular attention was given to those parameters and terms which controlled the behavior of the mathematical models. As terms were encountered which contributed little to the behavior of the reflectance changes, they were combined or eliminated, particularly if they required input about the details of the surface geometry. The simplified models were again tested against the empirical data to determine if the results had been degraded. Finally, after the models had been reduced to

require minimum surface parameter input data, they were tested against empirical reflectance data of real surfaces obtained for 441 different angular conditions for each surface during field experiments.

IV. THE MODEL

The basic equations describing each term of the shadow model are presented here with minimum explanation. Anyone interested in applying or testing the model is urged to obtain a copy of the detailed investigation report (Egbert, 1976), which contains a 50 page derivation of all equations.

The bidirectional reflectance distribution function was defined by Wolfe and Nicodemus (1965) and revised by Nicodemus (1970) as:

$$f_r(\theta_i,\phi_i;\theta_r,\phi_r) \equiv \frac{dL_r(\theta_r,\phi_r)}{L_i(\theta_i,\phi_i)d\Omega_i} \; sr^{-1} \tag{1}$$

where $d\Omega_i = \cos\theta_i d\omega_i$ (the projected solid angle)

L_i = radiance of the source, watts $m^{-2} sr^{-1}$

$dL_r(\theta_r,\phi_r)$ = differential radiance in the direction (θ_r,ϕ_r).

This is the function that describes the amount of energy (per unit projected solid angle) reflected from a surface toward a remote sensing device at an angle (θ_r,ϕ_r) from illumination by the sun at an angle (θ_i,ϕ_i). The primary objective of this study was to determine the feasibility of calculating the form of $f_r(\theta_i,\phi_i;\theta_r,\phi_r)$ from the statistical characteristics of shadow producing surface perturbations. In both cases θ represents an incidence angle measured from the normal to the surface and ϕ is azimuth angle measured in the plane of the surface. The subscript r represents reflectance or observation direction while i represents illumination direction. In later equations, a d subscript will be used to denote the difference angles between the two directions.

The intended use of the mathematical model developed in this investigation is to correct bidirectional reflectance measurements obtained at any arbitrary set of angles to some standard reflectance value. The choice of this standard reflectance is arbitrary so long as it is well defined. Since the mathematical model will be a correction function, it is only necessary to model the relative functional shape of f_r and not the absolute magnitude. The magnitude will be obtained from the measurement to be corrected. The standard reflectance chosen for the model development here is an "equivalent" Lambertian distribution factor f_L.

As defined here the equivalent Lambertian f_L for a non-Lambertian surface is the average value of all discrete values of f_r over a hemisphere when $\theta_i = 0$. If experimental data are in the form of percent reflectance calibrated relative to a standard diffuse target, then f_L can be approximated by:

$$f_L = \frac{1}{100} \frac{1}{N} \sum_{r=1}^{N} \%R(0^o,\theta_r) \tag{2}$$

A normalized function can be defined which relates the measured bidirectional reflectance to this equivalent Lambertian factor. This normalized function is the precise function that is derived in this investigation and can be defined by:

$$\Psi(\theta_i,\phi_i;\theta_r,\phi_r) \equiv \frac{f_r(\theta_i,\phi_i;\theta_r,\phi_r)}{f_L} \tag{3}$$

The relative percent reflectance from a particular surface at some set of angles can be predicted from:

$$\%R = 100 \; f_L \; \Psi(\theta_i,\phi_i;\theta_r,\phi_r) \tag{4}$$

The function Ψ represents a normalized bidirectional reflectance, and a single functional form can be used to describe categories of surfaces. Then, when the function is applied for a particular surface, it is converted to bidirectional reflectance or percent reflectance by multiplication by constants.

Since it is possible for the angular variations in path radiance to be of the same order of magnitude as the angular variations in reflectance, it is imperative that path radiance be taken into account in any calculation or measurement. Theoretical work is being conducted on the magnitude and variation of path radiance by Turner, et al. (1971) at the University of Michigan. They have developed a radiative transfer model which agrees quite well with experimental measurements. Therefore, it has not been an objective of this study to investigate the atmospheric contributions to the total radiance. Rather, those specific changes in the radiance reflected from the surface which are caused by the character of the surface have been the object of investigation. In operation, the model derived here for $\Psi(\theta_i,\phi_i;\theta_r,\phi_r)$ will most effectively be used in conjunction with an atmospheric correction model.

In order to allow maximum generalization within the limited scope of the study, a group of surface categories was methodically chosen to represent a broad spectrum of "real-world" surfaces. In all cases, the surface categories were chosen on the

basis of surface geometry and their texture as presented to the aerial remote sensing system. All model surface construction was performed using this group as a guide. Since it was not within the scope of the study to make different models to represent each surface in the group, two different simplified models were chosen. These were 1) spheres placed on a plane surface and 2) vertical cylinders placed on a plane surface. The equations presented here represent the spherical perturbation model specifically, although some terms are common to both. For a complete treatment of both models, see Egbert (1976).

A total of five specific reflectance terms can be defined which are used in the normalized bidirectional reflectance model.

(1) Lambertian reflectance from the illuminated and observed portion of a plane surface

(2) Lambertian reflectance from observed plane shadow area

(3) Lambertian reflectance from surface perturbations

(4) Forescatter specular reflectance from a plane surface

(5) Backscatter specular reflectance from surface perturbations

Additionally, a sixth factor is defined which is the heart of the shadow approach.

(6) Shadow function which determines the relative mixture of the five reflectance terms and acts as a modulation factor.

The total normalized bidirectional reflectance Ψ can be written as a superposition of these five terms.

$$\Psi = DRPL + DRSDW + DRS + DRSPF + DRSPB \qquad (5)$$

where: terms are in order as defined above and contain shadow function.

It will be shown that all five terms in equation 5 have a common factor of ΣR^2 (R = sphere radii). Further, all constants are defined from four surface parameters:

(1) dA = surface area being modeled

(2) TN = total number of perturbations in dA

(3) RM = mean perturbation radius

(4) f_L = equivalent Lambertian distribution factor

It should be noted that dA is a function of the sensor and f_L is estimated from reflectance measurements, so really only TN and RM need be estimated for unknown surfaces. It should also be noted that the factor ΣR^2 can be approximated by:

$$\sum_{j=1}^{TN} R^2 \cong TN\ RM^2 \qquad (6)$$

When this approximation is used, the entire reflectance model can be evaluated in terms of the four surface parameters listed above. The approximation was applied during the analysis of the laboratory experimental data and the results showed no noticeable degradation of model accuracy.

After evaluating Ψ for a specific surface, the relative percent reflectance is given by:

$$\%R(\theta_i,\phi_i;\theta_r,\phi_r) = 100\ f_L\ \Psi(\theta_i,\phi_i;\theta_r,\phi_r) \qquad (7)$$

For a constant intensity-collimated illumination source the irradiance per unit area incident upon the surface will vary as $\cos\theta_i$. Thus, the diffuse normalized bidirectional reflectance from the plane surface is given by:

$$DRPL = AILL\ \cos\theta_i \qquad (8)$$

Where, the fractional part of dA which is both illuminated and observed is:

$$AILL = \frac{dA - AVW - ASDW}{dA} \qquad (9)$$

And the total observed shadow area within dA is:

$$ASDW = \sum_{j=1}^{TN} \pi R^2 \left[(1-PROB)\sec\theta_i - \frac{AET}{\pi} \right] \qquad (10)$$

And, the viewing ellipse area for a constant angular field of view sensor is:

$$AVW = \sum_{j=1}^{TN} \pi R^2 \sec\theta_r (1-PROBV) \qquad (11)$$

Equations 8 through 11 define all of the terms in DRPL except PROB, PROBV, and AET. PROB is a function which describes the probability of perturbation shadows overlapping as the illumination incidence angle θ_i becomes increasingly larger.

PROB is defined by:

$$PROB = \frac{1}{1 + AR\ EXP(BR(90^\circ - \theta_i))}$$ (12)

and,

$$PROBV = PROB(\theta_r)$$ (13)

AR and BR are calculated through a linear least squares approximation of:

$$\ln\left(\frac{1}{PROB} - 1\right) = \ln(AR) + BR(90^\circ - \theta_i)$$ (14)

at four "critical angles" defined from the surface parameters TN and RM.

The first critical angle is defined as the angle at which the total shadow area is equal to one-fourth of dA.

$$CA1 = \cos^{-1}((4TN\pi RM^2)/dA)$$ (15)

This critical angle is approximately the angle at which the major axis of the shadow ellipse cast by a sphere of radius RM is equal to the mean spacing between spheres. Thus, overlap should just start to occur at CA1. PROB is defined as being equal to 0.05 at CA1. The second critical angle is defined as being the angle at which the total shadow area is equal to twice dA.

$$CA2 = \cos^{-1}((TN\pi RM^2)/(2dA))$$ (16)

At CA2 overlap should be near 100% and PROB is defined as being equal to 0.95. The third critical angle is defined as the average of the secants of the first two critical angles, and the fourth is defined as the arithmetic average of the first two. At CA3 PROB equals 0.5 and at CA4 PROB equals 0.25.

The final term in equations 8 through 11 is AET which is the amount of shadow area on the plane surface which is hidden from observation by the obstructing perturbations. For the spherical per-turbation model, both the shadow area and obstruc-ted area are ellipses. In this case, AET is the area of intersection of these two ellipses. The calculation of this area for any given set of angles is straightforward but the general integral equations are messy and lengthy, and so, they are not included here.

The next term in equation 5 is the Lambertian reflectance from the shadowed area and is given by:

$$DRSDW = \frac{ASDW}{dA}\ CS$$ (17)

where CS = a constant $\ll 1$

It was found empirically during the laboratory experiment phase of this study that a good estimate of CS is given by:

$$CS = (0.9\ f_L)^2$$ (18)

The diffuse reflectance from the perturbations within dA is given by:

$$DRS = \frac{2}{3\pi} \sum_{j=1}^{TN} R^2 \left[(\pi - \theta_d)\cos\theta_d + \sin\theta_d\right]$$ (19)

$$\frac{\sec\theta_r(1-PROBV)}{dA}$$

where θ_d = smallest angle between illumination direction and observation direction

The specular reflectance terms are similarly defined. The forescatter specular term is given by:

$$DRSPF = \frac{AILL\ RS(\theta_i)}{f_L} \frac{CH}{\sqrt{\pi}}\ EXP(-CH^2\theta_f^2)$$ (20)

$$+ \sum_{j=1}^{TN} R^2 \frac{RS(\theta_d)}{f_L}\ \sin^2(\theta_h)$$

Where θ_f = smallest angle between specular direction and observation direction

$$RS = \frac{RH + RV}{2}$$ (21)

RH and RV are the specular terms calculated from Fresnel's equations (Born and Wolf, 1959). It was found that the complex dielectric constant used to solve Fresnel's equations could be approximated by:

$$n \cong 1 + 10\ f_L^2$$ (22)

$$k \cong f_L + f_L^2$$ (23)

These values for n and k were used in the final form of the reflectance model and performed quite well. CH is a constant describing the angular spread of the specular term. It is convenient to describe CH in terms of a specular half power angle. Half power will occur at some angle θ_h so:

$$CH = \sqrt{\frac{-\ln(0.5)}{\theta_h^2}} = \sqrt{\frac{2.776}{\theta_h^2}} \qquad (24)$$

A value of 30° was used for θ_h for all surfaces in this study.

The last term in Ψ is the backscatter specular term given by:

$$DRSPB = \frac{AILL \ RS(\theta_i)}{f_L} \frac{CH}{\sqrt{\pi}} EXP(-CH^2\theta_d^2) \qquad (25)$$

$$(1-EXP(-CH^2\theta_f^2)) \ (1-EXP(-CH^2(\theta_d-\theta_f)^2))$$

These equations define the exact form of the shadow model normalized bidirectional reflectance for the ideal surface consisting of spherical perturbations on a plane. As can be seen from the equations, all equations can be evaluated from estimated values for only two surface geometrical parameters (TN, RM). A second set of equations (Egbert, 1976) define a similar model for the ideal surface consisting of cylindrical perturbations on a plane. These equations require values for three surface geometrical parameters where the mean sphere radius value is replaced by mean cylinder radius and height (RM, HM). Both models were evaluated during the course of this study as to their accuracy in predicting bidirectional reflectance variations for both ideal laboratory surfaces and non-ideal "real-world" surfaces.

V. EXPERIMENTAL RESULTS

The investigation consisted of two major parts, 1) laboratory experiments and 2) field experiments. During the laboratory experiments, nineteen artificial surfaces were constructed with precisely defined perturbation geometrical properties. Two different idealized perturbation shapes were used (spheres, and vertical cylinders). The field experiment part of the investigation tested the accuracy of the theoretical models when applied to five "real-world" surfaces. Two of the field experiment surfaces (asphalt parking lot, and plowed field) were appropriately described by the spherical perturbation model, while two others (Kentucky Fescue grass, and Buffalo grass) were appropriately described by the cylindrical perturbation model. The fifth surface (alfalfa) was not precisely described by either model, and was compared with both to determine the dependence of the

shadow approach on accuracy of perturbation shape description.

A. LABORATORY EXPERIMENTS

The two basic laboratory surface configurations consisted of a nearly Lambertian plane upon which two different types of nearly Lambertian perturbations were arranged (spheres and cylinders). The sphere radius and cylinder height distributions were Gaussian to simulate the size distributions of "real-world" surface perturbations. The density of perturbations per unit area (TN/dA) was varied while holding the Gaussian radius distribution constant for five different densities. Then, the variance of the size distribution (σ^2) was varied for a constant density to generate an additional four surfaces.

A theoretical reflectance value was calculated from Ψ for each sample surface at each of 432 different sets of angular conditions and compared with the measured value. Several statistics were calculated for each surface for an evaluation of the effectiveness of Ψ. The single best evaluating parameter was found to be the coefficient of determination r^2. Evaluation of detailed outputs for all surfaces showed no anomalies or errors of estimation which were not also exhibited by the summary statistics. Table 1 contains these statistics for the nine spherical perturbation model surfaces.

In order to determine which terms of Ψ contribute the most to accurately predicting angular reflectance variations, the data analysis procedure was repeated five more times. Each time one of the major terms of Ψ was deleted (see equation 5). The coefficients of determination for each of these cases are presented in Table 2.

As shown in this table, the coefficient of determination r^2 is very high for all surfaces. Examination of the detailed outputs revealed that both the calculated and measured reflectance values are dominated by the $\cos\theta_i$ term due to the decrease in illumination per unit surface area as θ_i is increased. This dominance masks the other variations and was subsequently removed to allow a closer analysis of the other terms. The results of this second analysis are presented in Tables 3 and 4. An examination of these tables shows that for constant illumination per unit surface area, Ψ still explains approximately 85% of the angular reflectance variations. Further, Table 4 clearly shows that the two most important terms are DRSPF and ASDW. For the surfaces with low perturbation densities, DRSPF is the relatively more important while for the high density surfaces, ASDW is the more important. This is not unexpected since the low density surfaces are smoother and by definition more specular. The large decrease in r^2 when ASDW is eliminated demonstrates the importance of considering shadows when calculating the bidirectional reflectance.

Tables 5 and 6 present the equivalent results for the cylindrical perturbation surfaces. One obvious trend can be observed in these tables. That is, r^2 is very low for the low perturbation density surfaces. This is particularly true for TN = 150 and 200. This is easily explained and in retrospect encouraging since for very small perturbation densities, the total shadow area is extremely small. Thus, a description of this surface based upon shadow parameters cannot be expected to produce good results. However, for the higher density surfaces, r^2 is higher and in most cases Ψ explains more than 80% of the variance in the measured bidirectional reflectance.

The effect of the shadow function is more vividly shown in Table 6, which presents r^2 for the calculations with individual terms removed from Ψ. When ASDW is removed from Ψ, the value of r^2 is a strong inverse function of TN. Conversely, when the forescatter specular term DRSPF is removed, r^2 decreases directly with TN. Thus, one important restriction of Ψ as derived in this investigation is demonstrated with these laboratory experiments. Ψ will not produce acceptable results when used to predict the bidirectional reflectance from smooth surfaces or surfaces with a low density of small perturbations.

B. FIELD EXPERIMENTS

The field reflectance measurements were obtained from color infrared photographs. The camera was mounted in a free swinging pivot platform adjusted so that it always pointed vertically. The pivot mount and camera were mounted on the end of an Elliott Hi-Reach truck boom and positioned at a height of 14.2 meters over the sample surface to be photographed. Photographs were taken at predetermined times for which the solar zenith angle was known. At each solar zenith angle, two photographs of the sample surface were taken, one with five gray cards in place on the ground and one without them. This provided a calibration for each data photograph.

Since it was the aim of the boom truck photographs to simulate data obtained from a typical aircraft remote sensing system, it was possible to use the average of many photographic resolution cell values to represent one airborne resolution cell value. The ground resolution of the boom photographs was approximately 4 mm. Although the resolution of airborne systems varies over a wide range, a resolution of 1.3 meters was chosen as representative of a large number of high resolution medium altitude systems.

Before the comparison between measured and calculated bidirectional reflectance could be made, it was necessary to estimate the required surface geometrical parameters (TN, RM, HM). For these detailed experiments, the parameters were derived from measurements of orthogonal close-up photographs obtained simultaneously with the field reflectance data.

Complete statistical summaries of the comparison between measured and calculated bidirectional reflectance (without $\cos\theta_i$ term) are shown in Tables 7 and 8. These show that independent of θ_i variations, the bidirectional reflectance function Ψ explains approximately 80 to 85 percent of the remaining reflectance variance for most of the surfaces. Overall, the spherical perturbation model appears to do slightly better, although the differences could easily be due to experimental error. It is significant that both perturbation models produce equivalent results for alfalfa which has a surface configuration not properly described by either model. This confirms the hypothesis that shadow produced angular reflectance variations are dependent on average perturbation size and density rather than on exact perturbation shape.

A comparison of Tables 7 and 8 shows that the two surfaces yielding the poorest results were Buffalo grass and plowed ground. These two surfaces both contain a very high density of shadow producing perturbations, and if this is the common cause of the poor results, there are two possible reasons. Either the overlap function does not adequately describe the shadow overlap for high perturbation densities, or the reflectance contribution from secondary scatter and skylight illumination is not adequately described. Errors in either one of these terms will affect high perturbation density surfaces more than low density surfaces.

An evaluation of the relative importance of each of the major Ψ terms (i.e., DRSPF, DRSPB, CS, DRS, and ASDW) was again performed for the field experiment data. The r^2 results of this evaluation are presented in Tables 9 and 10 for calculations without the $\cos\theta_i$ term. An examination of these tables shows that r^2 increases slightly for not only Buffalo grass and plowed ground but for all surfaces when the shadow illumination constant CS is set to zero. Thus, it can be concluded that the estimation used to calculate the shadow area reflectance contribution (equation 18) was in error. In fact, for the conditions existing at the time of field data acquisition (i.e., perfectly cloudless sky), the best results are obtained by assuming that the shadow contribution is zero.

Again, the field data analysis shows a dramatic decrease in r^2 when the shadow function is eliminated from Ψ. In all honesty, it must be stated that this change was so great that an examination of the model algorithms was made in search of errors which could have accentuated the drop in r^2. This examination revealed no errors or biases which could have produced the change. A detailed evaluation of complete outputs for each surface showed consistent behavior of all terms and residuals which is properly reflected by the values of r^2. Thus, it can be concluded that independent of the $\cos\theta_i$ term, 80 to 85 percent of the bidirectional reflectance variance can be explained by shadows.

VI. CONCLUSIONS

The results of this investigation demonstrate the validity of correcting for bidirectional reflectance variations on the basis of changing surface shadow area. The performance of the shadow models was evaluated as each of the major reflectance terms were singly deleted. In general, some decrease in model accuracy is experienced when any major term is deleted. However, a significant decrease in accuracy always occurs when the shadow function (ASDW) is deleted. Independent of the illumination angle cosine term, the models without the shadow function explain only 5 to 10 percent of the bidirectional reflectance variance. Alternatively, when any other major reflectance term is deleted, the models still explain 80 to 85 percent of the reflectance variance.

Further, it was established that shadow behavior is not greatly dependent upon the precise shape of surface perturbations. The two important shadow characteristics are 1) the total amount of shadow per unit area at any given illumination angle, and 2) the proportion of this shadow area which is observed at any given view angle. Both of these characteristics can be described in terms of an average perturbation density and average perturbation size. The analysis of the laboratory experiment data demonstrated that the estimated value for the product of these two parameters can be in error by 10 to 20 percent without significantly impacting the results. Further, the field experiments demonstrated that the shadow behavior of natural surfaces with irregularly shaped perturbations can be accurately described in terms of these two average parameters used in mathematical models derived for idealized perturbation shapes. The two models derived for different perturbation shapes (spherical, and cylindrical) both produced similar results when applied to a surface (alfalfa) with perturbation shapes unlike either original shape. Not only were the results similar for both models, but they were also similar to the results obtained for the exactly described laboratory surfaces. Thus, it is feasible to consider an operational correction function based upon shadowing, using average estimated surface parameters over broad areas of similar terrain.

VII. ACKNOWLEDGMENTS

VIII. REFERENCES

Allen, W., T. Gayle, and A. Richardson, (1970), Journal Optical Society of America, 60.

Born, M., and E. Wolf, (1959), Principles of Optics, The MacMillan Company, NYC, NY.

Egbert, D. D., (1976), "Determination of the Optical Bidirectional Reflectance from Shadowing Parameters," Ph.D. Dissertation, University of Kansas, March 1976, Available from University Microfilms, University of Michigan, Ann Arbor, Michigan.

Hapke, Bruce W., (1963), "A Theoretical Photometric Function for the Lunar Surface," Journal of Geophysical Research, vol. 68, no. 15, pp. 4571-4586, August 1963.

Hapke, Bruce W., and H. Van Horn, (1963), "Photometric Studies of Complex Surfaces, with Applications to the Moon," Journal of Geophysical Research, vol. 68, no. 15, pp. 4545-4570, August 1963.

Nicodemus, F. E., (1970), "Reflectance Nomenclature and Directional Reflectance and Emissivity," Applied Optics, vol. 9, pp. 1474-1475.

Smith, J. A., and R. E. Oliver, (1972), "Plant Canopy Models for Simulating Composite Scene Spectroradiance in the 0.4 to 1.05 Micrometer Region," Proceedings 8th International Symposium on Remote Sensing of Environment, University of Michigan, Ann Arbor, Michigan.

Suits, G. H., (1972), "The Calculation of the Directional Reflectance of a Vegetation Canopy," Remote Sensing of Environment, 2, pp. 117-125.

Turner, R. E., et al., (1971), "Importance of Atmospheric Scattering in Remote Sensing, or Everything You've Always Wanted to Know About Atmospheric Scattering but Were Afraid to Ask," Proceedings 7th International Symposium on Remote Sensing of Environment, University of Michigan, 17-21 May 1971, pp. 1651-1697.

Wolfe, W. L., and F. E. Nicodemus, (1965) in Wolfe, W. L., Handbook of Military Infrared Technology, Chapter 2, "Radiation Theory."
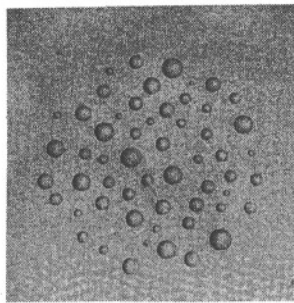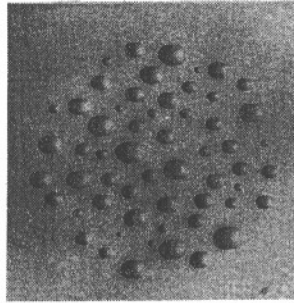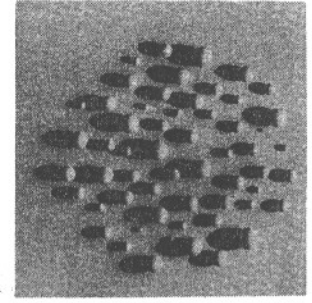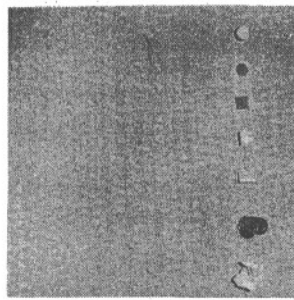
a) $\theta_i = 0°$ b) $\theta_i = 30°$ c) $\theta_i = 60°$
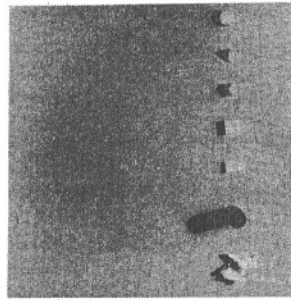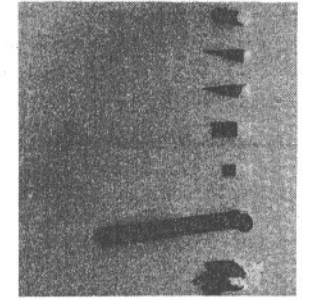
Figure 1. Examples of shadows projected by spheres upon a plane surface when illuminated by a collimated light source at three different incidence angles ($0°$, $30°$, $60°$).

a) $\theta_i = 0°$ b) $\theta_i = 30°$ c) $\theta_i = 60°$

Figure 2. Examples of shadows cast by irregularly shaped objects. From top to bottom objects in each photograph are: 1) vertical cylinder, 2) cone, 3) pyramid, 4) cube, 5) rectangular solid, 6) case for Polaroid print wiper, and 7) crumpled paper.

TABLE 1

SUMMARY OF RESULTS

SPHERICAL PERTURBATION SURFACES

TN	σ^2	*%R MEAN	*%R VAR.	COV.	RMS ERROR	AVG. ERROR		r^2
150	.034	12.25 / 11.93	59.14 / 55.03	56.93	.41	.32		.9959
200	.034	11.62 / 11.42	55.03 / 54.07	54.29	.57	.20		.9904
300	.034	11.75 / 11.50	59.77 / 57.63	58.61	.25	.26		.9972
350	.034	9.78 / 9.57	42.10 / 40.13	41.05	.18	.21		.9971
250	.012	11.52 / 11.31	55.77 / 54.44	54.96	.34	.21		.9948
250	.019	12.12 / 12.07	61.86 / 64.09	62.86	.24	.04		.9965
250	.034	10.46 / 10.30	45.79 / 43.69	44.63	.23	.16		.9959
250	.059	11.19 / 10.77	52.56 / 50.16	51.24	.42	.41		.9957
250	.082	12.26 / 11.93	63.40 / 64.75	64.01	.25	.33		.9980

All calculations made with TN x RM² including $\cos\theta_i$ variation.

*Upper Value = Calculated Data
 Lower Value = Measured Data

TABLE 2

RELATIVE IMPORTANCE OF REFLECTANCE MODEL TERMS

SPHERICAL PERTURBATION SURFACES

TN	σ^2	DRSPF =0	DRSPB =0	CS =0	DRS =0		ASDW =0
150	.034	.9813	.9923	.9959	.9959		.9945
200	.034	.9734	.9889	.9901	.9907		.9887
300	.034	.9763	.9953	.9965	.9973		.9916
350	.034	.9843	.9935	.9967	.9962		.9860
250	.012	.9680	.9936	.9940	.9954		.9895
250	.019	.9702	.9952	.9959	.9973		.9936
250	.034	.9805	.9938	.9959	.9962		.9929
250	.059	.9836	.9879	.9952	.9943		.9850
250	.082	.9788	.9943	.9975	.9980		.9932

All calculations made with TN x RM² including $\cos\theta_i$ variation.

Table Values = Coefficients of Determination r^2

TABLE 3
SUMMARY OF RESULTS
SPHERICAL PERTURBATION SURFACE

TN	σ^2	*%R MEAN	*%R VAR.	COV.	RMS ERROR	AVG. ERROR		r^2
150	.034	21.03 / 20.63	7.58 / 7.20	6.82	1.30	.40		.8526
200	.034	19.74 / 19.34	8.30 / 8.69	7.68	1.77	.39		.8187
300	.034	19.62 / 19.22	11.92 / 11.51	11.10	1.38	.39		.8982
350	.034	16.13 / 16.00	10.78 / 8.62	9.19	1.04	.12		.9082
250	.012	19.37 / 19.18	9.82 / 9.84	9.00	1.69	.19		.8384
250	.019	20.42 / 20.06	10.39 / 14.41	11.54	1.86	.36		.8890
250	.034	17.51 / 17.37	8.86 / 7.78	7.77	1.12	.14		.8748
250	.059	18.79 / 18.20	9.52 / 9.42	8.95	1.39	.59		.8929
250	.082	20.68 / 19.48	10.53 / 17.55	12.87	3.78	1.20		.8962

All calculations made with TN x RM² independent of cosθ₁ variation.

*Upper Value = Calculated Data
Lower Value = Measured Data

TABLE 4
RELATIVE IMPORTANCE OF REFLECTANCE MODEL TERMS
SPHERICAL PERTURBATION SURFACES

TN	σ^2		DRSPF =0	DRSPB =0	CS =0	DRS =0		ASDW =0
150	.034		.3624	.7149	.6679	.7918		.4391
200	.034		.3835	.8241	.7245	.8303		.1656
300	.034		.5857	.8686	.7069	.8175		.1499
350	.034		.7653	.8395	.7287	.7327		.0584
250	.012		.4133	.8121	.6122	.7658		.2602
250	.019		.4521	.9006	.7717	.8956		.1515
250	.034		.5631	.8342	.7427	.8162		.1142
250	.059		.7219	.7302	.6576	.7314		.1847
250	.082		.5403	.8789	.8615	.9418		.0898

All calculations made with TN x RM² independent of cosθ₁ variation.

Table Values = Coefficients of Determination r²

TABLE 5
SUMMARY OF RESULTS
CYLINDRICAL PERTURBATION SURFACES

TN	σ^2	*%R MEAN	*%R VAR.	COV.	RMS ERROR	AVG. ERROR		r^2
150	.55	16.99 / 17.06	6.68 / 4.10	3.16	4.44	-.07		.3657
200	.55	17.15 / 17.29	9.66 / 8.83	6.04	6.43	-.14		.4272
300	.55	15.65 / 16.07	15.05 / 9.52	9.88	4.97	-.43		.6821
350	.55	14.09 / 14.27	15.65 / 12.67	13.18	1.98	-.18		.8767
250	.19	16.96 / 16.85	12.80 / 12.88	10.68	4.32	.11		.6924
250	.31	16.84 / 16.81	12.71 / 10.81	10.65	2.21	.03		.8258
250	.55	16.56 / 16.64	12.51 / 10.07	10.11	2.36	-.08		.8121
250	.94	16.93 / 16.83	12.78 / 11.98	11.43	1.91	.10		.8530
250	1.30	16.95 / 17.12	12.79 / 10.39	10.26	2.69	-.17		.7916

All calculations made with TN x HM² independent of cosθ₁ variation.

*Upper Value = Calculated Data
Lower Value = Measured Data

TABLE 6
RELATIVE IMPORTANCE OF REFLECTANCE MODEL TERMS
CYLINDRICAL PERTURBATION SURFACES

TN	σ^2		DRSPF =0	DRSPB =0	CS =0	DRC =0		ASDW =0
150	.55		.2003	.2620	.1925	.2213		.1969
200	.55		.1602	.3993	.2518	.3203		.2516
300	.55		.5188	.6637	.5019	.5092		.0530
350	.55		.7750	.8588	.7495	.6860		.0005
250	.19		.6085	.6529	.5351	.5104		.0059
250	.31		.7055	.7753	.6575	.6215		.0066
250	.55		.7144	.7587	.6501	.6008		.0034
250	.94		.7526	.8066	.6893	.6562		.0010
250	1.30		.6715	.7415	.6116	.5878		.0152

All calculations made with TN x HM² independent of cosθ₁ variation.

Table Values = Coefficients of Determination r²

TABLE 7

SUMMARY OF RESULTS

SPHERICAL PERTURBATION SURFACES

SURF.	λ	*ΣR MEAN	*ΣR VAR.	COV.	RMS ERROR	AVG. ERROR		r²
ASPH. LOT	GREEN	20.38 / 20.01	25.33 / 31.19	26.13	4.39	.37		.8643
ASPH. LOT	RED	20.29 / 19.36	25.19 / 25.91	24.36	3.22	.93		.9098
ASPH. LOT	IR	20.15 / 18.83	24.99 / 32.01	25.96	6.82	1.33		.8426
ALF.	GREEN	5.12 / 4.91	2.21 / 2.31	2.14	.29	.23		.8943
ALF.	RED	3.17 / 2.80	.89 / 1.12	.88	.39	.37		.7732
ALF.	IR	10.35 / 9.40	7.90 / 10.62	8.66	2.09	.95		.8950
PLWD. FIELD	GREEN	11.88 / 11.89	10.17 / 15.51	11.03	3.61	-.01		.7772
PLWD. FIELD	RED	11.32 / 11.08	9.43 / 21.47	11.57	7.79	.24		.6617
PLWD FIELD	IR	15.86 / 14.47	15.63 / 24.28	17.34	7.16	1.39		.7918

Normalized data without $\cos\theta_i$

*Upper Value = Calculated Data
Lower Value = Measured Data

TABLE 8

SUMMARY OF RESULTS

CYLINDRICAL PERTURBATION SURFACES

SURF.	λ	*ΣR MEAN	*ΣR VAR.	COV.	RMS ERROR	AVG. ERROR		r²
K.F. GRASS	GREEN	11.65 / 12.57	16.23 / 15.49	14.16	4.26	-.93		.7968
K.F. GRASS	RED	9.45 / 10.01	11.20 / 10.75	9.93	2.40	-.56		.8188
K.F. GRASS	IR	13.87 / 14.01	21.89 / 17.61	17.73	4.04	-.14		.8156
ALF.	GREEN	4.82 / 5.33	3.67 / 3.86	3.51	.76	-.51		.8708
ALF.	RED	2.99 / 3.05	1.46 / 1.68	1.39	.36	-.06		.7905
ALF.	IR	9.75 / 10.22	13.33 / 17.05	14.17	2.26	-.47		.8831
BUF. GRASS	GREEN	9.25 / 10.78	15.99 / 19.22	14.46	8.63	-1.53		.6798
BUF. GRASS	RED	8.03 / 9.16	12.59 / 19.18	11.64	9.77	-1.13		.5604
BUF. GRASS	IR	13.25 / 14.66	28.31 / 31.37	23.94	13.75	-1.41		.6452

Normalized data without $\cos\theta_i$

*Upper Value = Calculated Data
Lower Value = Measured Data

TABLE 9

RELATIVE IMPORTANCE OF REFLECTANCE MODEL TERMS

SPHERICAL PERTURBATION SURFACES

SURF.	λ		DRSPF =0	DRSPB =0	CS =0	DRS =0		ASDW =0
ASPH. LOT	GREEN		.8805	.8149	.9080	.8972		.1194
ASPH. LOT	RED		.9164	.8826	.9408	.9264		.0802
ASPH. LOT	IR		.7902	.8410	.9114	.8838		.0572
ALF.	GREEN		.8877	.9006	.8987	.9361		.0926
ALF.	RED		.7782	.7738	.7774	.8336		.0582
ALF.	IR		.8924	.8983	.9091	.9254		.0202
PLWD. FIELD	GREEN		.7867	.7297	.7983	.8518		.0571
PLWD. FIELD	RED		.6892	.6293	.6899	.7286		.0493
PLWD FIELD	IR		.7936	.7722	.8612	.8405		.0331

Normalized data without $\cos\theta_i$

Table Values = Coefficients of Determination r²

TABLE 10

RELATIVE IMPORTANCE OF REFLECTANCE MODEL TERMS

CYLINDRICAL PERTURBATION SURFACES

SURF.	λ		DRSPF =0	DRSPB =0	CS =0	DRC =0		ASDW =0
K.F. GRASS	GREEN		.7961	.7652	.8389	.7768		.0174
K.F. GRASS	RED		.8186	.8024	.8468	.8075		.0170
K.F. GRASS	IR		.8069	.7907	.8617	.8154		.0332
ALF.	GREEN		.8725	.8709	.8761	.8705		.1050
ALF.	RED		.7957	.7898	.7943	.7729		.1453
ALF.	IR		.8952	.8719	.8976	.8803		.0669
BUF. GRASS	GREEN		.7021	.6490	.7290	.6614		.0006
BUF. GRASS	RED		.5858	.5332	.6055	.5355		.0087
BUF. GRASS	IR		.6769	.6005	.7336	.6255		.0005

Normalized data without $\cos\theta_i$

Table Values = Coefficients of Determination r²

Dr. Egbert has been with the Earth Resources
programming staff of GTE/IS at the Goddard
Institute for Space Studies for two years.
Prior to this, he spent one year with the Gen-
eral Electric Image Processing and Analysis
Laboratory in Beltsville, Maryland. He spent
several years with the University of Kansas
Center for Research, Inc. Remote Sensing Labor-
atory while attending graduate school. He
obtained his MSEE in 1971, and Ph.D.EE in 1976.